

Estimation of sea clutter inherent Doppler spectrum from shipborne S-band radar sea echo

Jin-Peng Zhang(张金鹏), Yu-Shi Zhang(张玉石), Xin-Yu Xu(许心瑜), Qing-Liang Li(李清亮), Jia-Ji Wu(吴家骥)

Citation: Chin. Phys. B . 2020, 29(6): 068402 . **doi:** 10.1088/1674-1056/ab888a
Journal homepage: http://cpb.iphy.ac.cn; http://iopscience.iop.org/cpb

What follows is a list of articles you may be interested in

Weak wide-band signal detection method based on small-scale periodic state of Duffing oscillator

Jian Hou(侯健), Xiao-peng Yan(闫晓鹏), Ping Li(栗苹), Xin-hong Hao(郝新红)

Chin. Phys. B . 2018, 27(3): 030702 . **doi:** 10.1088/1674-1056/27/3/030702

High resolution inverse synthetic aperture radar imaging of three-axis-stabilized space target by exploiting orbital and sparse priors

Jun-Tao Ma(马俊涛), Mei-Guo Gao(高梅国), Bao-Feng Guo(郭宝锋), Jian Dong(董健), Di Xiong(熊娣), Qi Feng(冯祺)

Chin. Phys. B . 2017, 26(10): 108401 . **doi:** 10.1088/1674-1056/26/10/108401

Compensation of body shake errors in terahertz beam scanning single frequency holography for standoff personnel screening

Wei Liu(刘玮), Chao Li(李超), Zhao-Yang Sun(孙兆阳), Yu Zhao(赵宇), Shi-You Wu(吴世有), Guang-You Fang(方广有)

Chin. Phys. B . 2016, 25(8): 088402 . **doi:** 10.1088/1674-1056/25/8/088402

Research on spatial-variant property of bistatic ISAR imaging plane of space target

Guo Bao-Feng, Wang Jun-Ling, Gao Mei-Guo, Shang Chao-Xuan, Fu Xiong-Jun

Chin. Phys. B . 2015, 24(4): 048402 . **doi:** 10.1088/1674-1056/24/4/048402

Modified GIT model for predicting wind-speed behavior of low-grazing-angle radar sea clutter

Zhang Yu-Shi, Zhang Jin-Peng, Li Xin, Wu Zhen-Sen

Chin. Phys. B . 2014, 23(10): 108402 . **doi:** 10.1088/1674-1056/23/10/108402

Estimation of sea clutter inherent Doppler spectrum from shipborne S-band radar sea echo*

Jin-Peng Zhang(张金鹏)[1,2,†], Yu-Shi Zhang(张玉石)[1], Xin-Yu Xu(许心瑜)[1], Qing-Liang Li(李清亮)[1], and Jia-Ji Wu(吴家骥)[2]

[1] China Research Institute of Radiowave Propagation, Qingdao 266107, China
[2] School of Electronic Engineering, Xidian University, Xi'an 710071, China

(Received 13 January 2020; revised manuscript received 26 March 2020; accepted manuscript online 12 April 2020)

Measurement of shipborne radar sea echo is instrumental in collecting the sea clutter data in open sea areas. However, the ship movement would introduce an extra Doppler component into the spectrum of the sea clutter, so the sea clutter inherent spectrum must be estimated prior to investigating the sea clutter Doppler characteristics from the shipborne radar sea echo. In this paper we show some results about a shipborne sea clutter measurement experiment that was conducted in the South China Sea in a period between 2017 and 2018; abundant clutter data have been collected by using a shipborne S-band clutter measurement radar. To obtain the sea clutter inherent Doppler spectrum from these data, an estimation method, based on the mapping relationship between the shipborne clutter spectrum and the inherent clutter spectrum, is proposed. This method is validated by shipborne clutter data sets under the same measuring conditions except for the ship speed. Using this method, the characteristics of the Doppler spectrum lineshapes in the South China Sea are calculated and analyzed according to different sea states, wave directions, and radar resolutions, which can be instrumental in designing the radar target detection algorithms.

Keywords: sea clutter, Doppler spectrum, shipborne radar, South China Sea

PACS: 84.40.Xb, 07.50.Qx, 02.50.Ey **DOI:** 10.1088/1674-1056/ab888a

1. Introduction

The Doppler spectrum of radar sea clutter refers to the Fourier transform of the autocorrelation function of the radar sea echo in a single radar range gate, that is, it is a power spectrum essentially.[1] The sea clutter spectrum is closely related to the scattering mechanism of sea wave,[2,3] thus it depends not only on the radar parameters but also on the spatial structure of the sea surface, which can be described by the wave height, wave direction, wave period, *etc*.[4] The different velocity components of the sea wave make the sea clutter spectrum have a mean shift and a bandwidth, which change with time variation and space variation of sea surface.

When searching for sea-skimming targets and during horizon searches, radars can encounter sea clutter in a variety of extreme weather conditions. For the coherent pulsed Doppler and MTI radars, the understanding of the sea Doppler characteristics is very conducible to predicting their performance correctly.[5,6] Therefore, continuous effort has been made to analyze the Doppler spectra of the sea clutter in various circumstances. Early in 1968, Pidgeon[7] investigated the Doppler dependence of radar sea clutter based on C-band clutter data and found the difference in Doppler characteristics between horizontal-polarization clutter and vertical-polarization clutter. Subsequently, Lee *et al.*[8] concentrated on exploring the different components of the Doppler spectra, which were induced by different sea surface scattering mechanisms. They have suggested that the Doppler spectrum of the radar sea clutter could be represented by the combination of several physically motivated basis functions, describing both Bragg and non-Bragg scattering mechanisms. Walker[9] presented a three-component model for the Doppler spectra of low grazing angle radar sea echoes, based on the findings of a laboratory wind-wave tank experiment. Lamont–Smith[4,10] focused on the explanation of the frequency and angle behaviors of the Doppler spectrum from the perspective of sea surface scattering mechanisms. In this century, Rosenberg and Watts *et al.*[11–14] have systematically analyzed the Doppler characteristics of the radar sea clutter measured under different radar parameters, different sea states, and different measuring geometries.

In general, the statistical properties of the wave height vary considerably in different maritime areas; thus, the Doppler characteristics of the radar sea clutter differ remarkably.[15] For example, according to our early qualitative research results of the sea clutter characteristic difference in various sea areas, it is indicated that the Doppler spectra in the South China Sea show larger bandwidths and have more sub-peaks than in Yellow Sea; this may be due to a larger depth and a faster current of the South China Sea. Therefore, it is of great significance to study the sea clutter Doppler spectra in

*Project supported by the National Natural Science Foundation of China (Grant No. 61801446).
†Corresponding author. E-mail: zhjinpeng@hotmail.com
© 2020 Chinese Physical Society and IOP Publishing Ltd

different maritime areas. From 2017 to 2018, a long-term experiment for multiple sea states, aiming to collect the radar sea clutter data of the South China Sea, was carried out by China Research Institute of Radiowave Propagation (CRIRP). In the experiment, a shipborne S-band clutter measurement radar (SSCMR) was fixed on the "Qiongsha 3" ship to measure the sea echo, and an ultrasound micrometeorological observation system was installed to collect the environmental data. The data collected provided a sound basis to investigate the Doppler characteristics of the radar sea clutter in the South China Sea.

This paper focuses on the experimental description of clutter collection and the estimation method of the sea clutter inherent Doppler spectrum. Because SSCMR measures the clutter data, the Doppler spectrum, if directly estimated from the clutter data, contains the Doppler component introduced by the ship movement. Therefore, to select the inherent Doppler spectrum of the sea clutter, which is mainly a result of the sea wave motion, the authors proposed a procedure in which used are the spectral formula of the sea clutter measured on ship platforms and a method of estimating the sea clutter inherent Doppler spectrum. Based on that procedure, the authors have analyzed the Doppler characteristics of the S-band sea clutter in the South China Sea for different sea states, wave directions, and radar resolutions. The results can be beneficial to designing the radar target detection algorithm in the corresponding sea area.

2. Clutter measurement experiment

2.1. Overview of experiment

The clutter measurement experiment has been conducted by CRIRP in a period between January 2017 and March 2018 in the South China Sea. To acquire the sea clutter data in the open sea, the SSCMR was installed on a supply ship "Qiongsha 3." This ship has been traveling between Hainan Province and Xisha Islands of China irregularly; therefore, the sea clutter was measured during the ship navigating.

The "Qiongsha 3" is 84-m-long and 13.8-m-wide, with a displacement of about 2500 tons, and it is shown in Fig. 1(a). The SSCMR was mounted on the bow port side, approximately 12 m above the sea surface; considering the height of the radar antenna, the total height of the radar was about 14.1 m above the sea surface. The depression angle of the radar was set to be 1°. Thus, according to the radar blind zone and the radar max power, the measurable grazing angle of the sea clutter was in a range from 0.3° to 1.1°, which is a relatively low grazing angle. The measurable azimuth angle of the sea clutter ranged from 190° to 350° (nose angle).

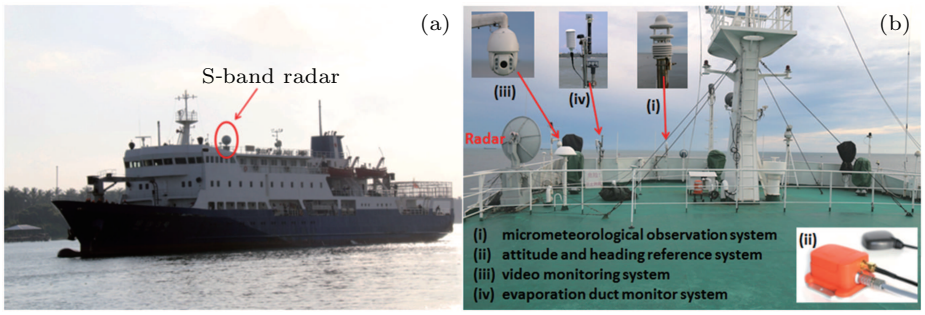


Fig. 1. Scene of shipborne sea clutter measurement system, showing (a) "Qiongsha 3" ship and (b) instruments mounted on deck.

The four other instruments installed on the ship deck as shown in Fig. 1(b), were used to collect assistant data necessary to support our investigation of the sea clutter characteristics. The instruments used were as follows: (i) an ultrasound micrometeorological observation system (LUFFT WS700) for collecting the meteorological data (*e.g.*, temperature and wind speed), (ii) an attitude and heading reference system (MTi-G) of the ship for recording attitude and navigation data of the ship, (iii) a video monitoring system of the radar to assist in setting the radar azimuth, and (iv) a shipborne evaporation duct monitor system for acquiring the propagation conditions of the radiowave around the radar. During the experiment, these systems were functioning simultaneously with the SSCMR, proving complete data set for the sea clutter study.

2.2. Radar system and data

The SSCMR system was equipped with a high-precision stabilization platform to maintain the stability of the radar beam pointing. By using a steerable pedestal, it was possible to conveniently steer the antenna in 360° azimuth and from 90° to −10° in elevation. The radar is a coherent, polarimetric system having 16 frequency points ranging from 3100 MHz to 3400 MHz, in steps of 20 MHz. In this study, we have used 3200-MHz frequency to measure the sea clutter. The radar design comprises four chirp bandwidths: 2.5, 5, 10, and 20 MHz, resulting in range resolutions of 60, 30, 15, and 7.5 m, respectively. Such a setup enables the investigation of the clutter in different radar resolutions. There are 794 range cells, corresponding to a maximum sampling distance of 5955 m. The

detailed list of SSCMR parameters can be found in Table 1.

Table 1. Main parameters of SSCMR.

Number	Parameter	Values
1	frequency	3.1 GHz to 3.4 GHz
2	polarization	HH
3	gain	56 dB
4	bandwidth	2.5 MHz, 5 MHz, 10 MHz, 20 MHz
5	PRF	500 Hz, 2 kHz, 5 kHz, 10 kHz
6	pulse width	3 μs
7	θ_{dB}	5.3°

θ_{dB} = 3-dB antenna beamwidth

During the two years of experimenting, having 18 voyages in total, many trials of the measurement have been carried out; the average radar measurement time was about 30 h per voyage. The acquired valid sea clutter data contained about 10784 sets or 6954 GB; the sea conditions varied from 2 to 5 (sea state scale, World Meteorological Organization). According to the sea state of each voyage and the number of data sets per voyage, the shares of the data volume with sea states 2, 3, 4, and 5 were about 33%, 23%, 32%, and 13%, respectively; there were relatively little data for sea state 5. The wave directions included upwave, downwave, and crosswave.

Figure 2 shows four typical range–pulse intensity plots of the sea clutter measured in different sea states; the radar parameters were the same. We see that the maximum measurable ranges of the sea clutter are different for the four sea states; as the sea state increases in the indicating number, the further sea echoes are received by the radar. This phenomenon complies with the known sea surface scattering mechanisms and indicates the validation of the measured clutter data.

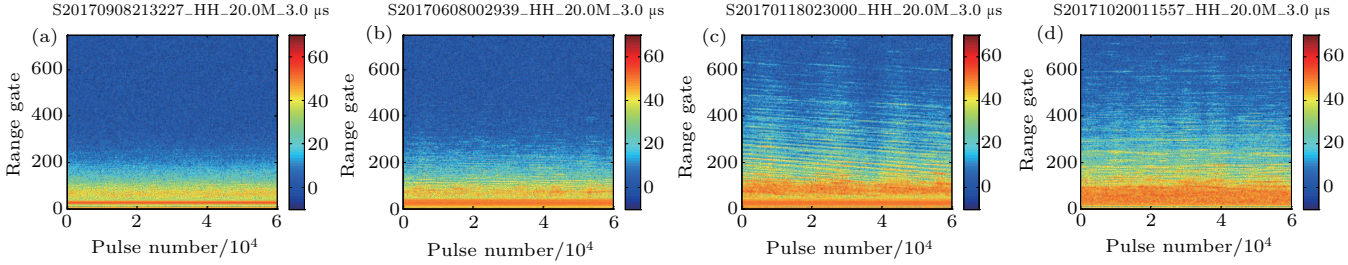


Fig. 2. Range–pulse intensity plots of sea clutter in sea state of (a) 2, (b) 3, (c) 4, and (d) 5.

3. Method of estimating sea clutter inherent spectra

3.1. Spectral formula of sea clutter measured on ship platform

In the case of a shipborne radar looking at the sea surface, if the position of the scatterer on the sea surface is represented by (r_l, θ_m), the velocity is represented by (v_{r_l}, v_{θ_m}), where (l, m) are the position indices in the slant-range and azimuth direction. The total sea clutter return measured by the radar in the spatial frequency (k_r, k_θ) domain can be written as

$$Y(k_r,k_\theta) = \sum_l \sum_m \sqrt{a(\theta_m)}\, y(r_l,\theta_m) \times \exp\left[-\mathrm{j}k_r\left(r_l - v_{r_l}\tau\right) - \mathrm{j}k_\theta\left(\theta_m - v_{\theta_m}\tau\right)\right], \quad (1)$$

where $a(\cdot)$ is the azimuthal two-way beam pattern of the radar antenna $y(\cdot)$ the amplitude of the radar backscatter, and τ the pulse repetition interval.

Based on the expression of the sea clutter intensity given by Eq. (1), in which the ship motion is considered, the corresponding power spectral density of the sea clutter is given by

$$\begin{aligned} P_{\mathrm{move}}(k_r,k_\theta) &= E\{Y(k_r,k_\theta)Y^*(k_r,k_\theta)\} \\ &= \sum_{l'}\sum_{m'}\sum_{l''}\sum_{m''}\sqrt{a(\theta_{m'})}\sqrt{a(\theta_{m''})} \\ &\quad \times E\{y(r_{l'},\theta_{m'})y^*(r_{l''},\theta_{m''})\} \\ &\quad \times \exp\left[-\mathrm{j}k_r\left(r_{l'} - v_{r_{l'}}\tau + \left(r_{l''} - v_{r_{l''}}\tau\right)\right)\right. \\ &\quad \left. -\mathrm{j}k_\theta(\theta_{m'} - v_{\theta_{m'}}\tau + (\theta_{m''} - v_{\theta_{m''}}\tau))\right]. \quad (2) \end{aligned}$$

Assuming that each return due to the radar backscatter is independent, the expectation in Eq. (2) can be simplified by

$$E\{y(r_{l'},\theta_{m'})y^*(r_{l''},\theta_{m''})\} = E\left\{|y(r_l,\theta_m)|^2\right\}. \quad (3)$$

Then, by using the Parseval's formula in the azimuth spatial domain k_θ, equation (2) can be rewritten as

$$\begin{aligned} &P_{\mathrm{move}}(k_r,k_\theta) \\ &= \mathrm{Im}\{a(\theta_m)\,|\theta_m\} \otimes_{k_\theta} \mathrm{Im}\left\{E\left\{|y(r_l,\theta_m)|^2\right\}|r_l,\theta_m\right\} \\ &= A(k_\theta) \otimes_{k_\theta} P_{\mathrm{clutter}}(k_r,k_\theta), \quad (4) \end{aligned}$$

where $A(k_\theta)$ is the antenna beam pattern in the azimuth spatial frequency domain, $P_{\mathrm{clutter}}(k_r,k_\theta)$ the sea clutter Doppler spectrum of a stationary platform, and $\otimes$ the convolution operator.

By transforming the spatial frequency k_θ into the Doppler frequency f, the power spectral density is given by Eq. (4) and can then be written as

$$P_{\mathrm{move}}(f) = A(f) \otimes_f P_{\mathrm{clutter}}(f). \quad (5)$$

Equation (5) shows that the sea clutter Doppler spectrum of a moving platform can be represented by the convolution of the sea clutter inherent Doppler spectrum and the radar antenna two-way beam pattern.

The antenna beam pattern is a function of the azimuth angle, which is in the Gaussian form and can be expressed as

$$A(f) = c_1 \cdot \exp\left[-\frac{(f-f_A)^2}{\sigma_A^2}\right], \tag{6}$$

where f_A and σ_A are the Doppler mean shift and Doppler bandwidth resulting from the movement of the radar platform, respectively, and c_1 is an energy conservation constant, since energy must not change after the convolution as shown in Eq. (5).

Figure 3 shows the geometry of calculating the Doppler components induced by the movement of the shipborne radar platform, where v_p is the velocity of the ship, φ is the angle between the moving direction of the ship and the projection of radar pointing direction (*i.e.*, the azimuth angle), θ is the grazing angle, and θ_b is the 3-dB azimuthal bandwidth of the radar beam.

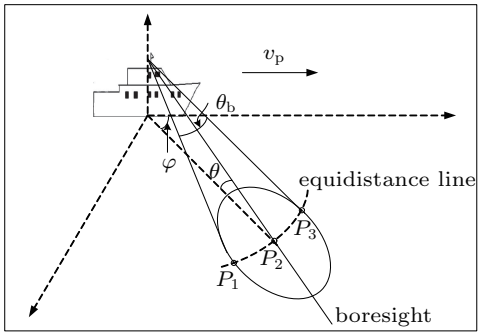


Fig. 3. Geometry of shipborne radar beam.

According to the geometry shown in Fig. 3, the Doppler shift induced by the ship movement can be calculated from[16]

$$f_A = \frac{2v_\mathrm{p}}{\lambda}\cos\varphi\cos\theta, \tag{7}$$

where λ is the electromagnetic wavelength.

In calculating the Doppler bandwidth induced by the ship movement, we consider three scattering points P_1, P_2, P_3 on the sea surface, with all points being equally distant from the radar as shown in Fig. 3. Points P_1 and P_3 are placed at the 3-dB edge of the antenna beam and P_2 is located at the antenna boresight. Because the three scattering points are located on the same wavefront, the radar backscatter at a certain time delay is the sum of the backscatter from these scattering points, but the angles between the ship motion direction and the backscattering directions are different slightly. Let P_2 have the azimuth angle φ, P_1 and P_3 be $\varphi \pm \theta_\mathrm{b}/2$; then the difference between the Doppler shift of the backscatter from P_1 and P_3 will be

$$\begin{aligned}\Delta f &= \frac{2v_\mathrm{p}}{\lambda}\left[\cos\left(\varphi-\frac{\theta_\mathrm{b}}{2}\right)-\cos\left(\varphi+\frac{\theta_\mathrm{b}}{2}\right)\right]\cos\theta \\ &= \frac{4v_\mathrm{p}}{\lambda}\sin\left(\frac{\theta_\mathrm{b}}{2}\right)\sin\varphi\cos\theta,\end{aligned} \tag{8}$$

which is the Doppler bandwidth induced by the ship movement. Equation (8) can have different simplified forms under different conditions. In the case of the radar antenna with a narrow beamwidth (for example, the beamwidth of SSCMR is 5.3° in this paper), if the azimuth angle of the radar beam is large enough, which makes the velocity vector not included in the main radar beam (*i.e.*, $|\varphi| > \theta_\mathrm{b}/2$), the expression of the Doppler bandwidth induced by the ship movement given by Eq. (8) can be simplified into

$$\sigma_A = \Delta f \approx \frac{2v_\mathrm{p}\theta_\mathrm{b}}{\lambda}\sin\varphi\cos\theta. \tag{9}$$

If the radar is forward looking which makes the velocity vector included in the main radar beam (*i.e.*, $|\varphi| < \theta_\mathrm{b}/2$), the simplified form of the Doppler bandwidth induced by the ship movement can be written as

$$\sigma_A = \Delta f \approx \frac{2v_\mathrm{p}}{\lambda}\left[1-\cos\left(\varphi+\frac{\theta_\mathrm{b}}{2}\right)\right]\cos\theta. \tag{10}$$

3.2. Estimation method

The sea clutter Doppler spectrum measured by a moving ship-based platform is widened by the aspect dependent Doppler spread due to the antenna beam pattern, so it is referred to as the sea clutter "spread" spectrum in this paper. The above subsection gives the mapping relationship between the spread spectrum and the sea clutter inherent spectrum determined by the wave movement. If the inherent spectrum is known, and the relevant parameters such as moving velocity, radar pointing direction, radar beamwidth, and grazing angle are given, the spread spectrum is easily calculated through the convolution given by Eq. (5). However, our purpose is to understand the characteristics of the sea clutter inherent Doppler spectrum based on the sea clutter data collected by a moving ship-based radar, so we need to obtain the inherent spectrum from the spread spectrum; this comprises an inverse process.

Based on Eq. (5), rather than trying to deconvolve the radar beam pattern from the sea clutter spread spectrum, we first introduce a parametric model to describe the lineshape of the sea clutter inherent spectrum. Then we fit the model to the sea clutter spread spectrum to determine the model parameters with the best fit by using the particle swarm optimization (PSO) algorithm. Afterward, the estimated parameters are used to characterize the inherent spectrum model estimating of the inherent spectrum. The estimation process is given in Fig. 4.

The ability of the Doppler model to describe the actual sea clutter Doppler spectrum determines the quality of the estimated shape of the inherent spectrum.[17] In the modeling of the sea clutter Doppler spectrum, the Walker model[9] and Ward model[18] are two widely accepted and used models. Here in this work, the Walker model is adapted to describe the

Doppler spectrum with the observation time longer than the period of the gravity sea waves (generally several seconds), which belongs to a long-time Doppler spectrum model. The Ward model is adapted for describing the Doppler spectrum with the observation time shorter than the period of the gravity sea waves but longer than the decorrelation times between the burst and whitecap scattering, which belongs to a short-time Doppler spectrum model.

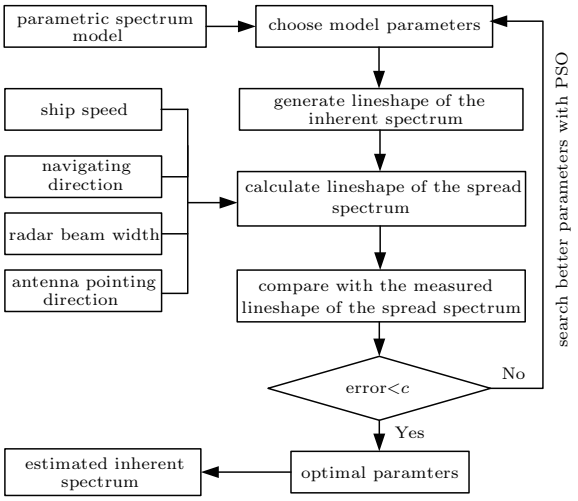


Fig. 4. Estimation process of sea clutter inherent spectrum.

The above two models have certain limitations in coping with the real sea clutter Doppler spectrum, so we use a suggested time-varying Doppler spectrum model for estimating the sea clutter inherent spectrum. This model is developed based on both the Walker model and Ward model. Thus, the real spectrum is described better by considering three different scattering mechanisms. The formula of the model can be written as

$$S_{\mathrm{HH}}(f,t\,|\Delta t) = I_{\mathrm{Bh}}(t\,|\Delta t)\cdot\Psi_{\mathrm{B}}(f)+I_{\mathrm{W}}(t\,|\Delta t)\cdot\Psi_{\mathrm{W}}(f) + I_{\mathrm{S}}(t\,|\Delta t)\cdot\Psi_{\mathrm{S}}(f), \tag{11}$$

$$S_{\mathrm{VV}}(f,t\,|\Delta t) = I_{\mathrm{Bv}}(t\,|\Delta t)\cdot\Psi_{\mathrm{B}}(f)+I_{\mathrm{W}}(t\,|\Delta t)\cdot\Psi_{\mathrm{W}}(f) \tag{12}$$

with

$$\Psi_{\mathrm{B}}(f)=\exp\left(-\frac{(f-f_{\mathrm{B}})^2}{w_{\mathrm{B}}^2}\right), \tag{13}$$

$$\Psi_{\mathrm{W}}(f)=\exp\left(-\frac{(f-f_{\mathrm{G}})^2}{w_{\mathrm{W}}^2}\right), \tag{14}$$

$$\Psi_{\mathrm{S}}(f)=\exp\left(-\frac{[f-(f_{\mathrm{G}}\pm\Delta f_{\mathrm{s}})]^2}{w_{\mathrm{S}}^2}\right), \tag{15}$$

where I_{B}, I_{W}, and I_{S} are the intensity of the Doppler components of Bragg, whitecap, and Burst scattering, respectively; w_{B}, w_{W}, and w_{S} are the corresponding Doppler bandwidths; f_{B} and f_{G} are the Doppler shifts corresponding to the Bragg resonance wave and phase velocity of gravity wave, respectively; Δf_{s} is an additional frequency shift. The detailed description of the model is given in Ref. [19].

In the estimation process of the sea clutter inherent spectrum, nine parameters are required to be optimized by PSO, they are I_{B}, I_{W}, I_{S}, w_{B}, w_{W}, w_{S}, f_{B}, f_{G}, and Δf_{s}. Their initial values are chosen as random numbers between $x_{\min}$ and $x_{\max}$, which represent the possible minimum and maximum values of each parameter. The possible values are determined by analyzing the real spread spectrum of the shipborne sea clutter.

3.3. Validation of estimation method

The method of estimating the sea clutter inherent Doppler spectrum was validated by the sea clutter data measured by SSCMR in the South China Sea in this section. The estimation process was as follows. First, we have chosen two sea clutter data sets with the same radar parameters, but one data set was acquired for the moving ship, and another data set was measured when the ship was static. To control the same sea conditions, the measurement time and sea area for the two data sets were made nearly equal. Secondly, based on the clutter data measured during the ship movement, we obtained the sea clutter spread spectrum by the Welch method, and then estimated the sea clutter inherent spectrum by using the method in this study. Finally, we have compared the estimated inherent spectrum with the Doppler spectrum yielded from the sea clutter data measured in the ship static state. If the two spectrum lineshapes have a good fit, it provee that the estimation method is valid.

Three validation tests were performed to evaluate the estimation method. Each test used two typical sets of clutter data: one corresponded to the static state of the ship and the other to the ship's moving state. The measuring conditions of all the test data are given in Table 2. The radar parameters are shown in Table 1. The measurement intervals between the two clutter data in three tests were 8 min, 10 min, and 7 min respectively, which ensured that the sea wave conditions are identical when they are collected. In Table 2, φ represents the angle between the ship movement direction and the radar pointing direction as shown in Fig. 3. As can be seen from the clutter maps in Table 2, diagonal stripes are visible if the ship is moving, which is due to the relative movement between the radar platform and the sea surface scatterers. The relative movement makes the sea waves look like sea targets in radar eyes.

The comparisons among the sea clutter Doppler spectra measured by a moving ship-based platform, by a stationary ship-based platform, and the estimated clutter inherent spectrum are shown in Fig. 5, taking one range gate for example. Good agreement occurs between the estimated inherent spectrum and the actual sea clutter spectrum (*i.e.*, the stationary platform clutter spectrum). The lineshapes of the clutter inherent spectrum are successfully reconstructed by the estimated ones.

Table 2. Measuring conditions of sea clutter data.

Test number	Data ID	Bandwidth/MHz	Range resolution/m	PRF	Sea state	$\varphi/(^\circ)$	Ship speed/m·s^{-1}	Clutter map
Test 1	Data 001	5	30	2000	4	138.76	5.95	
	Data 002	5	30	2000	4	—	0	
Test 2	Data 003	2.5	60	2000	3	42.79	7.48	
	Data 004	2.5	60	2000	3	—	0	
Test 3	Data 005	10	15	2000	4	142.07	5.01	
	Data 006	10	15	2000	4	—	0	

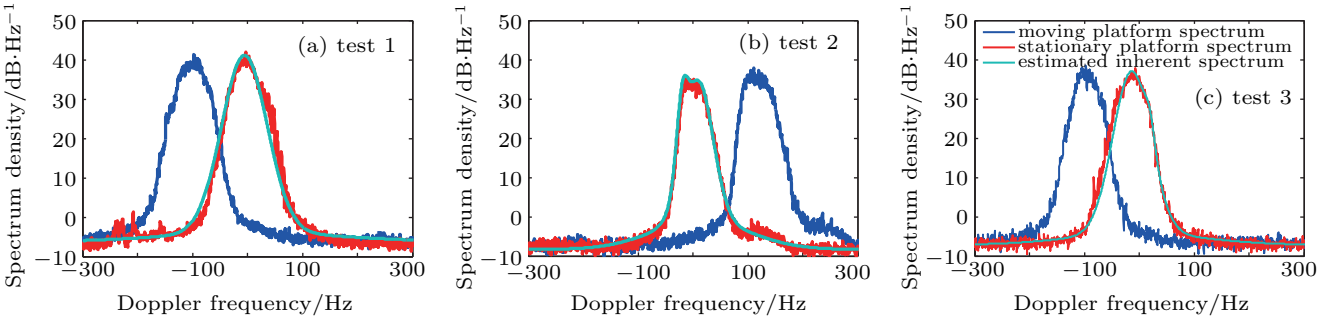


Fig. 5. Comparison between clutter inherent spectrum and stationary platform clutter spectrum for range gate 190.

Table 3. Estimation errors (in unit Hz) of Doppler parameters of clutter inherent spectrum.

Range gate	Test 1		Test 2		Test 3	
	Doppler mean shift	Doppler bandwidth	Doppler mean shift	Doppler bandwidth	Doppler mean shift	Doppler bandwidth
130	1.77	0.54	1.32	0.36	2.23	0.20
150	2.26	2.43	1.07	2.10	0.51	1.78
170	2.57	0.56	0.63	3.23	1.26	1.75
190	2.72	2.11	2.67	1.84	1.87	2.10
210	1.12	0.16	0.61	1.13	1.04	1.77
230	3.07	2.47	0.67	2.65	0.69	4.79
250	4.36	0.74	2.79	0.36	2.78	1.29
Mean	2.55	1.29	1.39	1.67	1.48	1.95

To evaluate the accuracy of the estimation method quantitatively, the estimation errors of the Doppler mean shift and bandwidth for the three tests were calculated, and are shown in Table 3. For each test, the inherent clutter spectra of 7 range gates were estimated, and the errors were counted. According to the results given in Table 3, it can be concluded that most of the mean estimation errors of the Doppler parameters are less than 2 Hz, except for the Doppler mean shift in test 1. Because the true values of these two Doppler parameters in S-band are on the order of tens of Hertz (refer to Fig. 5), the estimation errors shown in Table 3 are small and acceptable. This result validates the feasibility of the method of estimating the clutter inherent spectrum presented in this paper.

4. Characteristics of Doppler spectrum lineshapes

Based on the method of estimating the sea clutter inherent spectrum given in the previous section, the characteristics of the S-band sea clutter Doppler spectra in the South China Sea were investigated. For the signal detection in radar systems, the covariance matrix of the detection range cell based on the clutter data of neighborhood reference range cells must be typically estimated. Thus, the sea clutter is usually assumed to be spatially uniform, that is, the sea clutter in neighborhood range cells shares the same Doppler characteristics. However, due to the different wind conditions in different radar ranges and the

modulation effect of the slow varying wave components on the clutter power spectrum, the Doppler spectra for different radar range gates have different characteristics.[20] Therefore, firstly, the range-Doppler maps of the sea clutter in various conditions were analyzed to illustrate the variational manner of the spectrum lineshapes for different radar range gates, which is conducive to the estimation accuracy of the covariance matrix of the detection range cell. Then, the Doppler lineshapes for different sea states, different wave directions, and different radar range resolutions were compared and analyzed.

4.1. Different sea states

The typical range-Doppler maps of the sea clutter in the South China Sea estimated from the SSCMR clutter data in different sea states are presented in Fig. 6. By comparisons, the waves are of upwave direction for all sea states. The panels in the upper row are from the sea clutter "spread" spectra, and those in the lower row are from the sea clutter inherent spectra. As shown in the spread spectrum images, the Doppler mean shifts are about −100 Hz in sea states 2, 3, and 5. However, the shift is about +100 Hz for the sea state 4 spectrum. The spectra shapes indicate that in the two of the cases, the radar was looking backward and forward, relative to the ship moving direction. Although the Doppler shifts of the spread spectra exhibit different signs in the two cases, still all Doppler shifts of the corresponding inherent spectra share the same plus sign, proving that the wave directions are upwave for all the sea states, which coincide with the measuring condition of the clutter data.

By comparing the Doppler spectrum intensities shown in Fig. 6, as the sea state increases, the Doppler intensity of the clutter inherent spectrum clearly increases distinctly, indicating the growth of the clutter energy. As can be observed in the Doppler map, the Doppler intensity decreases as the range increases. Otherwise, by analyzing the fluctuation of the Doppler intensity *versus* range, the Doppler intensity clearly varies more significantly on the right side of the spectrum peak, and the spectrum spikes occur in these Doppler bins. This phenomenon can be attributed to the upwave conditions of the sea clutter data.

Figure 7 shows a typical comparison of the inherent spectrum lineshapes of the South China Sea in different sea states. The lineshapes are corresponding to the sea clutter data of the range gates 180 and 230 as shown in Figs. 6. Evidently, the Doppler mean shift and the bandwidth increase as the sea state increases; only the difference in Doppler mean shift is not remarkable for sea state 2 nor sea state 3, which is because the significant wave heights are similar for these clutter data. Moreover, as the sea state increases, the spectrum peak becomes increasingly complex, trending to exhibiting bimodal lineshapes.

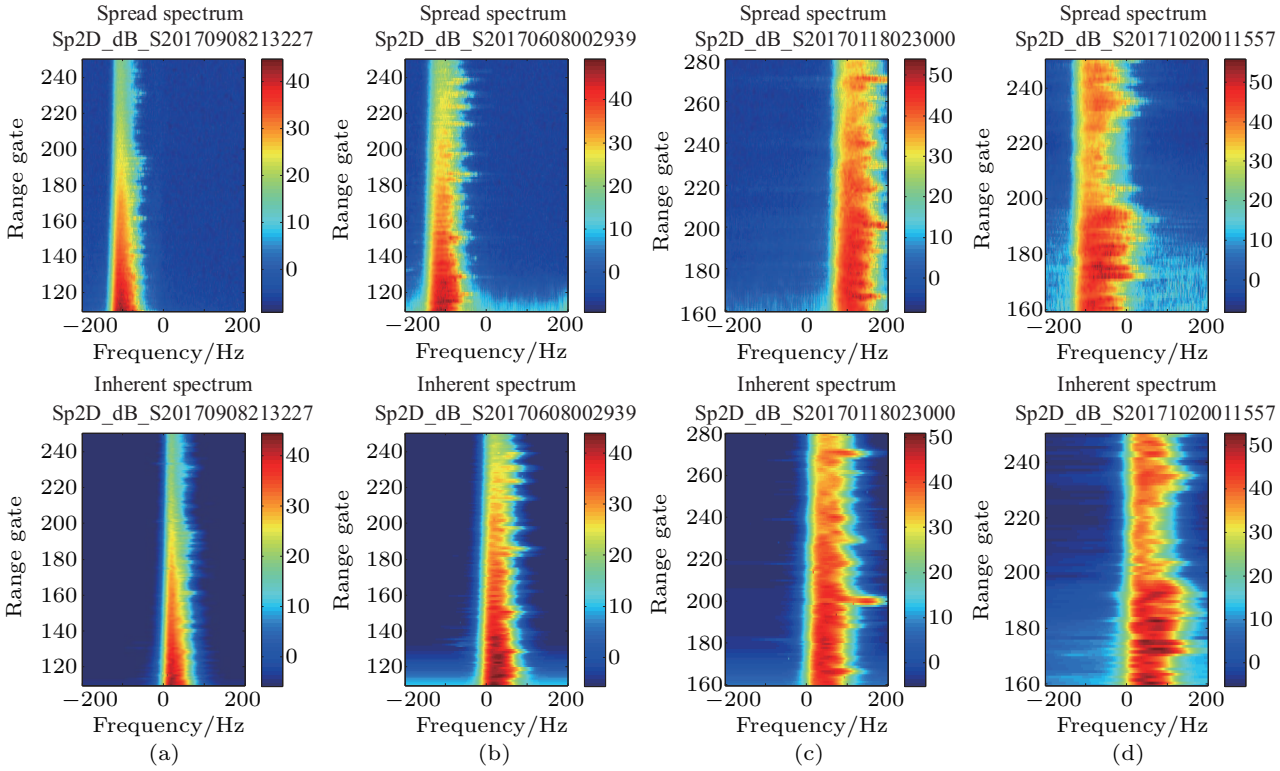


Fig. 6. Range–Doppler maps of sea clutter in the South China Sea in sea states of (a) 2, (b) 3, (c) 4, and (d) 5.

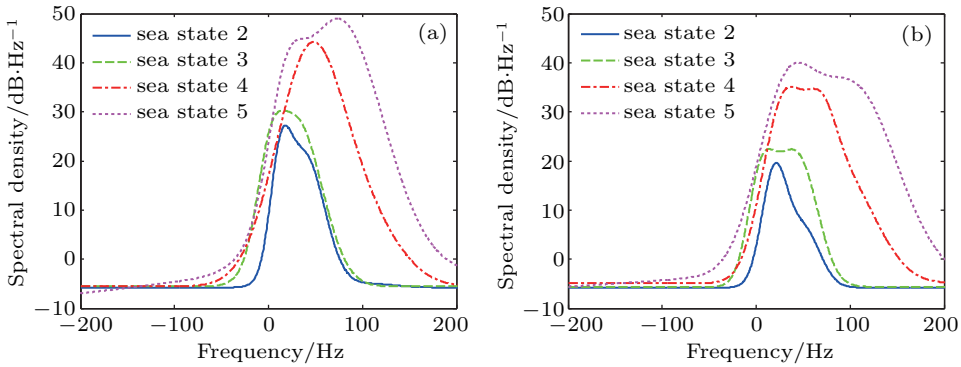


Fig. 7. Comparison of inherent spectrum lineshapes of sea clutter in the South China Sea in different sea states: (a) gate = 180 and (b) gate = 230.

4.2. Different wave directions

Figure 8 shows the typical range–Doppler maps of the sea clutter in the South China Sea for three different wave directions. The sea states were 3 in all these cases. From the sea clutter inherent spectra displayed in the lower row, we can observe that the wave direction has a significant influence on the Doppler mean shift, resulting in positive shift for upwave, negative shift for downwave, and near-zero shift for crosswave conditions. The Doppler mean shift is not strictly equal to zero for a crosswave case because the angle between the radar looking direction and the wave direction is not always equal to 90°. Further, as observed in the fluctuations of the spectrum intensity at each Doppler bin, under the upwave condition, the fluctuation is more intense for the Doppler bins on the side of positive Doppler shifts. However, under the downwave condition, the fluctuation is more intense on the side of negative Doppler shifts. Under the crosswave conditions, the fluctuations are comparable on both sides of the spectrum peak.

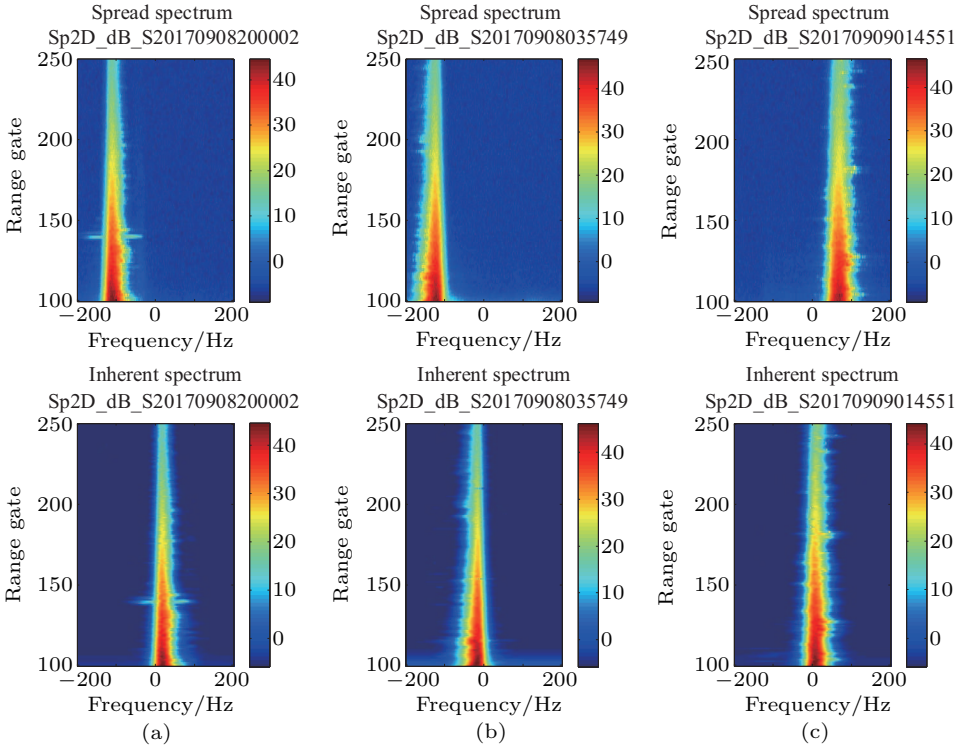


Fig. 8. Range–Doppler maps of sea clutter in the South China Sea in (a) upwave, (b) downwave, and (c) crosswave directions.

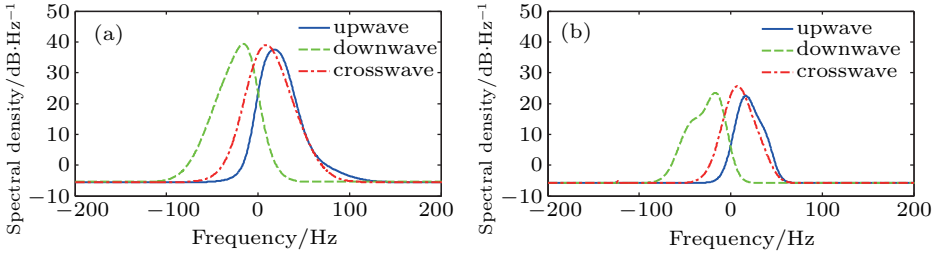


Fig. 9. Comparisons of sea clutter spectrum lineshapes of the South China Sea in different wave directions: (a) gate = 120 and (b) gate = 200.

To illustrate the influence of wave direction on Doppler spectrum lineshape, figure 9 shows the lineshapes of the sea clutter inherent spectra obtained from the data of range gates 120 and 200 as shown in Fig. 8. Evidently, the symmetry of the lineshape and the Doppler mean shift are distinctly affected by the wave direction, but the influence on the Doppler bandwidth is not significant.

4.3. Different radar resolutions

The typical range–Doppler maps of the sea clutter in the South China Sea, estimated from the SSCMR clutter data with four different radar range resolutions, are displayed in Fig. 10. The sea conditions are sea state 3 and upwave. By comparing the Doppler maps in the four cases, the noticeable influence of the radar resolution can be observed in the variation degree of the spectrum intensity. When the resolution is 7.5 m, because the radar resolution cell is too small to cover a complete sea wave, the sea surface structure between different resolution cells changes remarkably; thus, the radar received clutter energy in each adjacent range gate exhibits considerable fluctuation. As a result, the Doppler spectrum exhibits a rapid fluctuation *versus* range. However, as the radar resolution decreases, the fluctuation of the spectrum weakens. When the resolution is 60 m, the Doppler spectrum exhibits a stable change with range increasing, owing to the small difference in clutter intensity between adjacent radar resolution cells, and this is further because a radar resolution cell contains multiple sea waves.

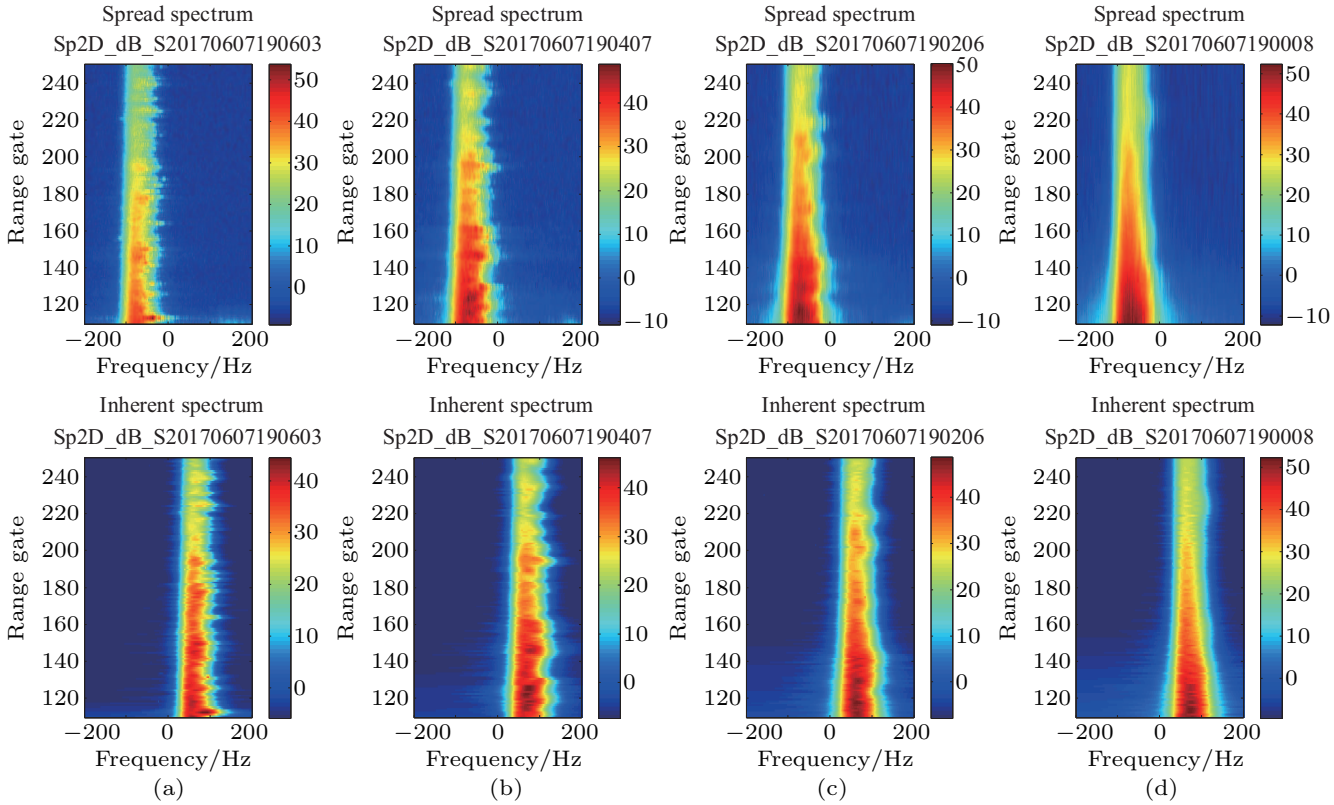


Fig. 10. Range–Doppler maps of sea clutter in the South China Sea for radar range resolutions of panel (a) 7.5 m, panel (b) 15 m, panel (c) 30 m, and panel (d) 60 m.

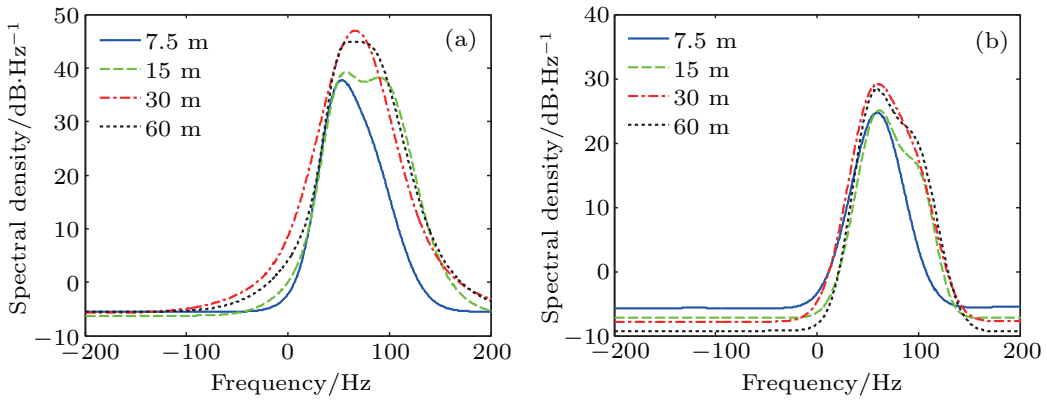


Fig. 11. Comparisons of sea clutter spectrum lineshape of the South China Sea in different radar range resolutions: panel (a) gate = 130 and panel (b) gate = 220.

Based on the clutter data of range gates 130 and 220 shown in Figs. 10, figure 11 displays the comparisons of the lineshape of the sea clutter inherent spectrum among different radar range resolutions. For the radar resolution of 7.5 m, the Doppler bandwidth is relatively small, but for the other three cases, the Doppler bandwidths are larger and have approximately the same value. This phenomenon illustrates that as the radar resolution decreases to a critical value, knowing that a resolution cell can contain multiple sea waves and consequently the speed component of the sea wave reaches a stable state, the Doppler bandwidth does not change any further. For the Doppler mean shift, the influence of the radar resolution is not clear.

4.4. Doppler spectrum parameters

In addition to the characteristics of Doppler spectrum lineshapes, the quantitative results of the Doppler spectrum parameters, including the Doppler mean shift and bandwidth, play an important role in suppressing the clutters of radar target detection. Based on the estimated inherent Doppler spectrum lineshapes from the large data sets in the experiment, we calculate and analyze the characteristics of the two Doppler spectrum parameters in the South China Sea, and the statistical results are shown in Table 4. The corresponding grazing angle is 0.8°, and the results are the mean values under different conditions.

Table 4. Statistics of Doppler spectrum parameters of radar sea clutter.

Sea state	Wave direction	Doppler mean shifts/Hz				Doppler bandwidth/Hz			
		60 m	30 m	15 m	7.5 m	60 m	30 m	15 m	7.5 m
2	upwave	20.9	22.4	22.2	23.0	11.5	12.0	12.6	13.4
	downwave	−17.7	−17.0	−17.8	−17.6	7.5	7.4	8.0	8.9
3	upwave	27.1	30.8	25.7	28.4	14.9	15.5	14.9	15.3
	downwave	−21.9	−20.1	−21.3	−21.4	8.5	8.8	9.5	11.4
4	upwave	42.2	40.4	39.4	39.3	18.2	17.9	17.5	17.4
	downwave	−37.8	−36.8	−35.7	−33.9	13.0	12.7	13.1	13.6
5	upwave	49.0	46.4	46.4	44.9	24.6	23.9	23.5	23.5
	downwave	−46.5	−46.6	−47.4	−47.8	16.1	16.9	16.8	17.0

According to the results given in Table 4, we can conclude as follows.

(i) Under all measuring conditions, the variation trends of the Doppler mean shift and bandwidth as a function of sea state are very evident. The higher the sea state, the larger the absolute values of the two parameters are, which is in accordance with the scenario for faster wave speed and more complex sea wave components in higher sea states.

(ii) The sea wave direction has a distinct influence on the Doppler mean shift and bandwidth. The Doppler mean shift is positive in upwave and negative in downwave conditions, which meets the physical mechanism of the sea clutter Doppler spectrum. The Doppler bandwidth is wider for upwave and narrower in downwave cases, which indicates that there are more components of sea wave velocity in upwave conditions than in downwave conditions.

(iii) The radar range resolution has a little influence on the mean value of the Doppler mean shift and bandwidth. However, as shown in Fig. 10, we can deduce that with the increase of the radar range resolution, the distribution of the Doppler shift and bandwidth of sample becomes wider, that is, the variance of the sample increases. This is because the variation of the Doppler spectrum structure with range is more distinct for a smaller radar resolution.

5. Conclusions

The Doppler characteristics of the S-band radar sea clutter in the South China Sea are presented and analyzed in this study based on the clutter data measured by SSCMR deployed on “Qiongsha 3” ship in a period of 2017–2018. A novel estimation method used to acquire the sea clutter inherent Doppler spectrum from the shipborne clutter data is introduced, and good agreement between its results and the actual sea clutter spectrum (*i.e.*, the spectrum from motionless ship) is obtained. Further, using this method, the Doppler spectrum lineshapes in the South China Sea are compared and analyzed in sea states, wave directions, and radar resolutions. The dependence of the Doppler lineshape on these measuring conditions is also presented.

Acknowledgment

The authors would like to express their sincere thanks to the members of the clutter research group in China Research Institute of Radiowave Propagation for their work on the sea clutter experiment.

References

[1] Lee P H Y, Barter J D, Beach K L, *et al.* 1995 *J. Geophys. Res.* **100** 2591

[2] Walker D 2000 *IEE Proc. Radar Sonar & Navig.* **147** 114

[3] Xiong G, Zhang S N and Zhao H C 2014 *Acta Phys. Sin.* **63** 150503 (in Chinese)
[4] Lamont-Smith T 2004 *IEE Proc. Radar Sonar & Navig.* **151** 291
[5] Farshchian M 2017 *IEEE Geosci. Remote Sensing Letters* **14** 232
[6] Xing H Y, Zhang Q, Xu W 2015 *Acta Phys. Sin.* **64** 110502 (in Chinese)
[7] Pidgeon V W 1968 *J. Geophys. Res.* **73** 1333
[8] Lee P H Y, Barter J D, Lake B M *et al.* 1998 *IEE Proc. Radar Sonar & Navig.* **145** 135
[9] Walker D 2001 *IEE Proc. Radar Sonar & Navig.* **148** 73
[10] Lamont-Smith T 2008 *IET Radar Sonar & Navig.* **2** 97
[11] Rosenberg L 2014 *IEEE Trans. Aerosp. Electron. Syst.* **50** 406
[12] Watts S, Rosenberg L, Bocquet S, *et al.* 2016 *IET Radar Sonar & Navig.* **10** 24
[13] Watts S, Rosenberg L, Bocquet S, *et al.* 2016 *IET Radar Sonar & Navig.* **10** 32
[14] Rosenberg L and Bocquet S 2018 *International Confernece on Radar*, Brisbane, QLD, Australia
[15] Johnsen T 2015 *IEEE Radar Conf.*, Johannesburg, South Africa **109**
[16] Richards M A 2005 *Fundamentals of Radar Signal Processing* (The McGraw-Hill Companies, Inc.)
[17] Bocquet S 2018 *International Conference on Radar*, Brisbane, QLD, Australia
[18] Ward K D, Tough R J A and Watts S 2013 *Sea clutter: Scattering, the K-distribution and radar performance*, 2nd. edn. (London: The Institution of Engineering and Technology)
[19] Zhang J P, Zhang Y S, Li Q L, *et al.* 2018 *Acta Phys. Sin.* **67** 034101 (in Chinese)
[20] Javier C M, Javier G M, Alberto A, *et al*. 2011 *IEEE Transactions on Aerospace and Electron System* **47** 1880